Sum-Rate Maximization for Intelligent Reflecting Surface Assisted Terahertz Communications

Yijin Pan, Kezhi Wang, Cunhua Pan, Huiling Zhu and Jiangzhou Wang, *Fellow, IEEE*

***Abstract*—In this paper, an intelligent reflecting surface (IRS) is deployed to assist the terahertz (THz) communications. The sum-rate of user equipments (UEs) is maximized while guaranteeing the rate requirement of each UE. A block coordinate searching (BCS) algorithm is proposed to jointly optimize the IRS's coordinates, phase shifts, THz sub-bands allocation and power control. Specifically, the relaxation with penalties based (RPB) algorithm is developed to obtain feasible coordinates of the IRS and guarantee the monotonicity of objective value. In addition, the IRS phase shifts are formulated as closed-form expressions with introduced pricing factors. Simulation results show that the proposed scheme can significantly enhance system performance.**

***Index Terms*—Intelligent reflecting surface (IRS), Terahertz (THz) communication, Reconfigurable intelligent surface (RIS).**

I. Introduction

The terahertz (THz) band wireless transmission has been envisioned as a promising solution to meet the ultra-high data rate requirements of emerging applications such as the virtual reality (VR) service. However, due to its ultra-high frequency, the propagation at THz is short-ranged and susceptible to blockages, and this issue becomes severe with indoor furniture layout [1]. Recently, intelligent reflecting surface (IRS), also known as reconfigurable intelligent surface (RIS), has been proposed to reconfigure wireless propagation environment to enhance transmission performance, such as the simultaneous wireless information and power transfer (SWIPT) system [2] and multicell network [3] through careful design of the phase shifts of the IRS. Due to its capability of constructing an alternative communication link, the IRS is very attractive for 6G mobile network [4], especially for the applications in THz communications that are sensitive to blockages. However, the study on IRS-aided THz communications is still in its infancy [5]–[7] and numerous important issues are not yet addressed.

The sum-rate performance of the IRS-aided THz communication was studied in [5]–[7]. In fact, the bandwidth offered by the THz band ranges from 0.1 THz to several THz. Due to the propagation loss and high molecular absorption in the THz band, severe path loss peaks appear in several frequencies. Hence, the total bandwidth may be divided into several sub-bands with different bandwidths [8]. Nevertheless, how to utilize multiple sub-channels for effective THz transmission has not been addressed in the above-mentioned studies [5]–[7]. Although [9] has provided an efficient IRS-assisted OFDM UAV transmission scheme, the unique channel characteristics of the THz band were not considered. Furthermore, when the IRS is exploited to assist THz transmission, the delay and phase shift on each sub-band is dependent on its central frequency. As a result, adjusting IRS phase shifts for simultaneous use of multiple radio frequencies is quite challenging.

Meanwhile, the path loss peaks in THz band depend on the link distances, which highly rely on the location of IRS. So far, for many indoor applications, the locations of user equipments (UEs), such as the IoT monitors, can be predicted according to the indoor layout and the historical statistics of UEs' locations [10]–[12]. Consequently, the information of UEs' location can be exploited at the AP to decide the optimal deployment of the IRS. In addition, the path loss of the sub-band varies with the communication distance [13], [14], so that the optimization of the IRS's location has the potential to further boost the system performance. Therefore, it is imperative to jointly optimize the deployment of IRS, the reflecting phase shift, along with the sub-band allocation to enhance the IRS-assisted THz transmission. Unfortunately, this issue has not yet been addressed in the existing literature.

Against the above background, in this paper, the sum-rate maximization problem is investigated for a THz indoor transmission system assisted by the RIS. To solve the formulated nonconvex problem, a block coordinate searching (BCS) algorithm is proposed to jointly optimize the IRS's coordinates, reflecting phase shifts, THz sub-bands allocation and power control. To deal with the intractable optimization of the IRS's coordinates, the relaxation with penalties based (RPB) algorithm is proposed to guarantee the solution's feasibility and the monotonicity of objective value. To optimize the IRS's reflecting coefficients, the sub-gradient descent (SGD) algorithm is proposed, where the IRS's phase shifts are expressed in closed forms with the pricing factors. Simulation results are provided for performance evaluation.

II. System Model

As shown in Fig. 1(a) , an access point (AP) operates in THz frequency to support indoor applications such as indoor surveillance or augmented reality (AR) services. Suppose that the AP serves U UEs and the UE set is denoted by $\mathcal{U}$. The locations of UEs can be traced or predicted according to the indoor home furniture layout. Consequently, the location information of UEs is assumed to be available at the AP, and the coordinates of UE u is denoted by $\boldsymbol{w}_u = [x_u, y_u, z_u]^T$.

The line-of-sight (LOS) link from the AP to a given area may be blocked by obstacles such as the pillar or wall, and this area is assumed to be rectangular with length L and width W. The IRS is installed on the ceiling with height H. Suppose that the IRS is a uniform planar array (UPA) with $N = N_x \times N_y$ passive reflecting elements, and the separation between

Corresponding authors: Kezhi Wang and Cunhua Pan. Y. Pan and C. Pan are with the National Mobile Communications Research Laboratory, Southeast University, Nanjing 211111, China. Email: panyj@seu.edu.cn. K. Wang is with the Department of Computer and Information Sciences, Northumbria University, UK. Email: kezhi.wang@northumbria.ac.uk. J. Wang and H. Zhu are with the School of Engineering and Digital Arts, University of Kent, UK. Email: J.Z.Wang@kent.ac.uk, H.Zhu@kent.ac.uk.

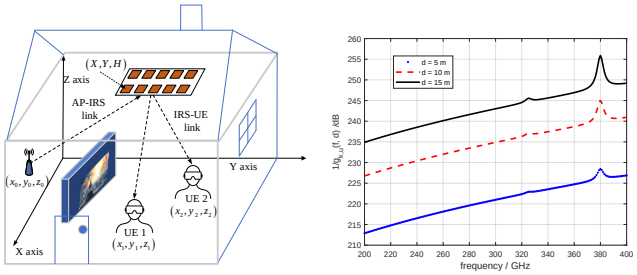

(a) The transmission scenario. (b) Path loss $1/|g_{u,i}(f_i,d_u)|^2$.

Fig. 1: Transmission scenario and THz channel path loss.

adjacent IRS elements is denoted by Δ. The coordinates of the first reflecting element is denoted by $\boldsymbol{l}_1 = [X, Y, H]^T$, where "$T$" stands for matrix transpose. As a result, the coordinates of the n-th reflecting element is $\boldsymbol{l}_n = [X+(n_x-1)\Delta, Y+(n_y-1)\Delta, H]^T$, where $n = (n_y-1)N_x+n_x$, $n_x = 1, \cdots, N_x$, and $n_y = 1, \cdots, N_y$. Similar to [2], [3], [15], assume that the IRS reflecting elements share the same amplitude value of one but have different phase shifts. Let ϕ_n denote the phase shift of the n-th reflecting element of the IRS, which can be carefully adjusted by an IRS controller.

Assume that the THz channel can be perfectly estimated according to the ray-tracing method [14], [16]. According to the ray-tracing method, the propagation effects includes spreading, molecular absorption, reflection, and scattering [17]. However, in THz band, reflection and scattering play insignificant roles in the received signal power due to the high THz frequencies [18], [19]. Consequently, similar to [1], [20], we neglect the effects of reflections, scattering, and only consider the LOS components of the AP-IRS link and the IRS-UE links, which can be perfectly estimated as functions with respect to the frequency f_i, the molecular absorption, and the link distance.

The coordinates of the AP is denoted by $\boldsymbol{w}_0 = [x_0, y_0, z_0]^T$. For the AP-IRS link, we define transmit steering vector as $\boldsymbol{e}_t(f, \boldsymbol{l}) = \left[1, e^{-j\theta_1(f,\boldsymbol{l})}, \cdots, e^{-j\theta_N(f,\boldsymbol{l})}\right]$. The phase $\theta_n(f, \boldsymbol{l})$ represents the phase difference of the incoming signal with radio frequency f to the n-th reflecting element relative to the first element, and it is given by

$$\theta_n(f, \boldsymbol{l}) = \frac{2\pi f}{c} \frac{\boldsymbol{r}_0(\boldsymbol{l})^T}{|\boldsymbol{r}_0(\boldsymbol{l})|}(\boldsymbol{l}_n - \boldsymbol{l}_1), \tag{1}$$

where $|\boldsymbol{x}|$ represents the Euclidean norm of vector $\boldsymbol{x}$, $\boldsymbol{r}_0(\boldsymbol{l}) = [X - x_0, Y - y_0, H - z_0]^T$, and c is the light speed.

For the link from the IRS to UE u, we define the receiving steering vector as $\boldsymbol{e}_{u,r}(f, \boldsymbol{l}) = \left[1, e^{-j\vartheta_1(f,\boldsymbol{l})}, \cdots, e^{-j\vartheta_N(f,\boldsymbol{l})}\right]$. Then, the phase difference of the signal received with radio frequency f at UE u from the n-th reflecting element relative to the first element is

$$\vartheta_n^u(f, \boldsymbol{l}) = \frac{2\pi f}{c} \frac{\boldsymbol{r}_u(\boldsymbol{l})^T}{|\boldsymbol{r}_u(\boldsymbol{l})|}(\boldsymbol{l}_n - \boldsymbol{l}_1), \tag{2}$$

where $\boldsymbol{r}_u(\boldsymbol{l}) = [x_u - X, y_u - Y, z_u - H]^T$.

In the THz band, the absorbent molecules composited in the transmission medium cause several peaks of channel attenuation, as shown in Fig. 1(b), where with the atmospheric pressure 101325 Pa, 50% relative humidity, and 23°C. As a consequence, the total bandwidth needs to be divided into several sub-bands. Let f_i denote the central frequency of the i-th sub-band, and $\lambda_i = \frac{c}{f_i}$ is the wavelength. The set of sub-bands is denoted by $\mathcal{I}$, and the number of sub-bands is assumed to be I. According to [16], [21] and the Fraunhofer distance [22], the cascaded channel gain of the AP-IRS-UE u link on the i-th sub-band is

$$g_{u,i}(f_i, \boldsymbol{l}) = \frac{\sqrt{G_t}\sqrt{G_r}\lambda_i}{8\sqrt{\pi^3} r_u^s(\boldsymbol{l})} e^{-j\frac{2\pi}{\lambda_i} d_u(\boldsymbol{l})} e^{-\frac{1}{2}K(f_i)d_u(\boldsymbol{l})}, \tag{3}$$

where G_t and G_r respectively represent the transmit and receive antenna gain, $r_u^s(\boldsymbol{l}) = |\boldsymbol{r}_0(\boldsymbol{l})||\boldsymbol{r}_u(\boldsymbol{l})|$, $d_u(\boldsymbol{l}) = |\boldsymbol{r}_0(\boldsymbol{l})| + |\boldsymbol{r}_u(\boldsymbol{l})|$, and $K(f_i)$ is the overall absorption coefficient of the medium on the i-th sub-band. Then, the reflecting channel of AP-IRS-UE u link can be expressed as

$$h_{u,i}(f_i, \boldsymbol{\Phi}, \boldsymbol{l}) = g_{u,i}(f_i, d_u)\boldsymbol{e}_{u,r}(f_i, \boldsymbol{l})^H \boldsymbol{\Phi} \boldsymbol{e}_t(f_i, \boldsymbol{l}), \tag{4}$$

where $\boldsymbol{\Phi} = \text{diag}(e^{j\phi_1}, \cdots, e^{j\phi_N})$.

To evaluate $K(f_i)$, we adopt a simplified molecular absorption coefficient model for 200 – 400 GHz frequency band [23], which has two major absorption peaks at about 325 GHz and 380 GHz. This simplified model only depends on the volume mixing ratio of water (humidity) μ_w and frequency f (Hz):

$$K(f) = \frac{A(\mu_w)}{B(\mu_w) + \left(\frac{f}{100c} - 10.835\right)} + \frac{C(\mu_w)}{D(\mu_w) + \left(\frac{f}{100c} - 12.664\right)} + p_1 f^3 + p_2 f^2 + p_3 f + p_4, \tag{5}$$

where $A(\mu_w) = 0.2205\mu_w(0.1303\mu_w + 0.0294)$, $B(\mu_w) = (0.4093\mu_w + 0.0925)^2$, $C(\mu_w) = 2.014\mu_w(0.1702\mu_w + 0.0303)$, $D(\mu_w) = (0.537\mu_w + 0.0956)^2$, $p_1 = 5.54 \times 10^{-37}\text{Hz}^{-3}$, $p_2 = -3.94 \times 10^{-25}\text{Hz}^{-2}$, $p_3 = 9.06 \times 10^{-14}\text{Hz}^{-1}$, and $p_4 = -6.36 \times 10^{-3}$. The volume mixing ratio of water vapour μ_w is evaluated as $\mu_w = \frac{\phi_H}{100}\frac{p_w(T, p_{ss})}{p_{ss}}$, where ϕ_H and p_{ss} (measured in hectopascal) respectively represent the relative humidity and the pressure. The saturated water vapour partial pressure $p_w(T, p_{ss})$ also depends on temperature T (measured in °C), according to Buck equation [23], which is calculated as $p_w(T, p_{ss}) = 6.1121(1.0007 + 3.46 \times 10^{-8} p_{ss}) \exp\left(\frac{17.502T}{240.97+T}\right)$.

Similar to [14], we assume that each sub-band is less than coherence bandwidth, so that narrowband communication on each sub-band can be achieved [24]. Let B_i denote the bandwidth of the i-th sub-band, the obtained transmission rate of UE u on the i-th sub-band is given by

$$R_{u,i}(f_i, p_i^t, \boldsymbol{\Phi}, \boldsymbol{l}) = B_i \log\left(1 + \frac{p_i^t}{\sigma_i^2}|h_{u,i}(f_i, \boldsymbol{\Phi}, \boldsymbol{l})|^2\right), \tag{6}$$

where p_i^t represents the transmit power and σ_i^2 is the noise power on the i-th sub-band, respectively.

III. Problem Formulation

Let the binary variable $\alpha_{u,i}$ indicate that UE u is assigned with i-th sub-band. Assume that each sub-band is only allocated to one UE. Then, we have

$$C1: \alpha_{u,i} \in \{0, 1\}, \sum_{u \in \mathcal{U}} \alpha_{u,i} = 1, i \in \mathcal{I}, u \in \mathcal{U}. \tag{7}$$

The transmit power is limited by maximum power p_{max} as

$$C2: \sum_{i \in \mathcal{I}} p_i^t \leq p_{max}. \tag{8}$$

In addition, for the IRS reflecting coefficient $e^{j\phi_n}$, we have

$$C3: 0 < \phi_n < 2\pi, 1 \le n \le N. \tag{9}$$

Furthermore, we have the following restriction on the deployment of IRS coordinates $\boldsymbol{l} = [X, Y]$ as

$$C4: 0 \le X \le W, 0 \le Y \le L. \tag{10}$$

Also, the rate requirement should be satisfied for each UE as

$$C5: \sum_{i\in\mathcal{I}} \alpha_{u,i} R_{u,i}(f_i, p_i^t, \boldsymbol{\Phi}, \boldsymbol{l}) \ge R_u^{th}, \forall u \in \mathcal{U}. \tag{11}$$

We aim to maximize the sum-rate of UEs by jointly optimizing the IRS's coordinates $\boldsymbol{l}$, sub-bands allocation $\alpha_{u,i}$, the transmit power p_i^t and the phase shift of IRS $\boldsymbol{\Phi}$. Then, we formulate the following optimization problem as

$$\max_{\boldsymbol{\Phi}, \alpha_{u,i}, p_i^t, \boldsymbol{l}} \quad R_s = \sum_{u\in\mathcal{U}} \sum_{i\in\mathcal{I}} \alpha_{u,i} R_{u,i}(f_i, p_i^t, \boldsymbol{\Phi}, \boldsymbol{l}) \tag{12a}$$

$$\text{s.t.} \quad C1 - C5. \tag{12b}$$

Note that it is difficult to find a feasible solution for initialization due to constraint $C5$. As a result, we introduce auxiliary variables $\{\beta_u\}$ to relax constraint $C5$. We then reformulate Problem (12) as:

$$\max_{\mathcal{X}} \; R_s(\delta_{u,i}) - W_\beta \sum_{u\in\mathcal{U}} (\beta_u - 1)^2 \tag{13a}$$

$$\text{s.t.} \; \sum_{i\in\mathcal{I}} B_i \log(1 + \delta_{u,i}) \ge \beta_u R_u^{th}, \forall u \in \mathcal{U}, \tag{13b}$$

$$\delta_{u,i} = \alpha_{u,i} p_i^t |h_{u,i}(f_i, \boldsymbol{\Phi}, \boldsymbol{l})|^2 \sigma_i^{-2} \tag{13c}$$

$$C1 - C4,$$

where $R_s(\delta_{u,i}) = \sum_{u\in\mathcal{U}} \sum_{i\in\mathcal{I}} B_i \log(1 + \delta_{u,i})$, and $\mathcal{X} = \{\alpha_{u,i}, p_i^t, \boldsymbol{\Phi}, \boldsymbol{l}, \beta_u, \delta_{u,i}\}$ and W_β is the introduced weight. It is observed that Problem (13) is always feasible, as β_u can be initialized as $\beta_u < 1$ to relax constraint (13b). However, to maximize the objective function (13a), the optimal value of β_u converges to $\beta_u^* = 1$.

IV. Solution Analysis

To solve Problem (12), we decouple it into three subproblems: 1) optimization of IRS's coordinates; 2) IRS phase shifts optimization; 3) sub-band allocation and power control.

A. IRS Coordinates Optimization

In this section, IRS's coordinates are optimized with given $\boldsymbol{\Phi}$, β_u, $\alpha_{u,i}$ and p_i^t. Let $\mathcal{I}_u$ represent the set of sub-bands that are allocated to UE u. By introducing auxiliary variables $\{t_{u,i}\}$, the optimization problem of IRS's coordinates is

$$\max_{\boldsymbol{l}, t_{u,i}} \; R_s(t_{u,i}) = \sum_{u\in\mathcal{U}} \sum_{i\in\mathcal{I}_u} B_i \log(1 + t_{u,i}) \tag{14a}$$

$$\text{s.t.} \; p_i^t |h_{u,i}(\boldsymbol{l})|^2 \ge t_{u,i} \sigma_i^2, \forall u \in \mathcal{U}, i \in \mathcal{I}_u, \tag{14b}$$

$$\sum_{i\in\mathcal{I}_u} B_i \log(1 + t_{u,i}) \ge \beta_u R_u^{th}, \forall u \in \mathcal{U}, \tag{14c}$$

$$t_{u,i} \ge 0, \forall u \in \mathcal{U}, i \in \mathcal{I}, C4.$$

It is observed that Problem (14) is difficult due to the nonconvex constraint (14b). For ease of exposition, we introduce auxiliary variables $r_0 = |\boldsymbol{r}_0(\boldsymbol{l})|$, $r_u = |\boldsymbol{r}_u(\boldsymbol{l})|$ and define function $f_{u,i}(r_0, r_u) = (r_0 r_u)^{-1} e^{-K_i(r_u + r_0)}$, where $K_i = K(f_i)/2$. Then, the left hand side of (14b) is represented as

$$p_i^t |h_{u,i}(\boldsymbol{l})|^2 = f_{u,i}(r_0, r_u) \underbrace{\left(\frac{p_i^t \sqrt{G_t} \sqrt{G_r} \lambda_i}{8\sqrt{\pi^3}} \boldsymbol{e}_{u,r}(f_i, \boldsymbol{l})^H \boldsymbol{\Phi} \boldsymbol{e}_t(f_i, \boldsymbol{l}) \right)^2}_{\upsilon_{u,i}(\boldsymbol{l})} \tag{15}$$

Note that the challenge of (15) is dominated by term $\upsilon_{u,i}(\boldsymbol{l})$, which involves many periodic cosine components with respect to the sub-bands' index and UE's index. Consequently, we utilize the solution obtained at the (n)-th iteration denoted as $(\boldsymbol{l}^{(n)}, t_{u,i}^{(n)})$ to simplify Problem (14).

With the IRS's coordinate $\boldsymbol{l}^{(n)}$, term $\upsilon_{u,i}(\boldsymbol{l})$ is replaced with the constant $\upsilon_{u,i}(\boldsymbol{l}^{(n)})$, constraint (15) can be simplified as

$$p_i^t |h_{u,i}(\boldsymbol{l})|^2 \approx f_{u,i}(r_0, r_u) \upsilon_{u,i}(\boldsymbol{l}^{(n)}). \tag{16}$$

The first-order derivative of $f_{u,i}(r_0, r_u)$ is given by

$$\nabla_{u,i}(x) = \frac{\partial f_{u,i}(x, y)}{\partial x} = -x^{-2} y^{-1} e^{-K_i(x+y)} (K_i x + 1).$$

Directly substituting (16) into the left hand side of (14b) still results a nonconvex problem. It can be verified that the Hessian matrix of $f_{u,i}(r_0, r_u)$ is positive-definite. As a result, $f_{u,i}(r_0, r_u)$ is convex with respect to (r_0, r_u), and its first-order Taylor-expansion can be utilized to simplify (14b) as

$$\begin{aligned} &\upsilon_{u,i}(\boldsymbol{l}^{(n)}) (\nabla_{u,i}(r_0^{(n)})(r_0 - r_0^{(n)}) \\ &+ \nabla_{u,i}(r_u^{(n)})(r_u - r_u^{(n)}) + f_{u,i}(r_0^{(n)}, r_u^{(n)})) \ge t_{u,i} \sigma_i^2, \end{aligned} \tag{17}$$

where $r_0^{(n)} = |\boldsymbol{r}_0(\boldsymbol{l}^{(n)})|$ and $r_u^{(n)} = |\boldsymbol{r}_u(\boldsymbol{l}^{(n)})|$ are the distances of AP-IRS link and IRS-UE u link at the (n)-th iteration, respectively. Then, Problem (14) is simplified into

$$\max_{r_0, r_u, \boldsymbol{l}, t_{u,i}} \quad R_s(t_{u,i}) \tag{18a}$$

$$\text{s.t.} \; R_s(t_{u,i}) \ge R_s(t_{u,i}^{(n)}) \tag{18b}$$

$$|\boldsymbol{r}_0(\boldsymbol{l})| \le r_0, |\boldsymbol{r}_u(\boldsymbol{l})| \le r_u, \tag{18c}$$

$$(17), (14c), C4.$$

Constraint (18b) is introduced to guarantee that the obtained objective value $R_s(t_{u,i})$ increases with iterations. Note that Problem (18) is convex, and it can be easily solved by CVX.

However, note that (17) is not exactly equivalent to (14b), we introduce the following penalties to ensure that the obtained $(\boldsymbol{l}^*, t_{u,i}^*, r_0^*, r_u^*)$ is a feasible solution to Problem (14). Define $t_{u,i}^l = f_{u,i}(r_0^*, r_u^*) \upsilon_{u,i}(\boldsymbol{l}^*)$, and

$$\gamma_u = \beta_u R_u^{th} - \sum_{i\in\mathcal{I}_u} B_i \log\left(1 + \delta_i t_{u,i}^l\right) \tag{19}$$

$$\gamma = R_s(t_{u,i}^{(n)}) - R_s(t_{u,i}^l). \tag{20}$$

If $\gamma_u > 0$, the obtained solution $(\boldsymbol{l}^*, t_{u,i}^*, r_0^*, r_u^*)$ cannot satisfy all the constraints of Problem (14). Also, if $\gamma > 0$, the obtained objective value $R_s(t_{u,i}^l)$ by $(\boldsymbol{l}^*, t_{u,i}^*, r_0^*, r_u^*)$ is less than that of the n-th iteration. Then, the right hand sides of (14c) and (18b) are respectively modified as

$$\tilde{R}_u^{th} = \beta_u R_u^{th} + \text{sgn}(\gamma_u)\epsilon_u, \tag{21}$$

$$\tilde{R}_s(t_{u,i}) = R_s(t_{u,i}^{(n)}) + \text{sgn}(\gamma)\epsilon, \tag{22}$$

where function $\text{sgn}(x) = 1$, if $x > 0$, otherwise if $x \leq 0$, $\text{sgn}(x) = 0$. Then, constraints (14c) is updated by replacing $\beta_u R_u^{th}$ with $\tilde{R}_u^{th}$ in (21), and constraints (18b) is updated by replacing $R_s(t_{u,i}^{(n)})$ with $\tilde{R}_s(t_{u,i})$ in (22). Also, the solution $(\boldsymbol{l}^*, t_{u,i}^*, r_0^*, r_u^*)$ to Problem (18) with the modified constraints should be updated accordingly. If $\gamma_u \leq 0, \forall u$ and $\gamma < 0$, the finally obtained solution $(\boldsymbol{l}^*, t_{u,i}^*, r_0^*, r_u^*)$ satisfies all the constraints of Problem (14), and IRS's coordinate for the $(n+1)$-th iteration is obtained as $\boldsymbol{l}^{(n+1)} = \boldsymbol{l}^*$. Moreover, the obtained objective $R_s(t_{u,i})$ is guaranteed to be non-decreasing with iterations.

Based on the above discussions, we provide the details for solving Problem (14) in Algorithm 1.

Algorithm 1 Relaxation with Penalties Based (RPB) Algorithm to Solve Problem (14)

Initialize $\boldsymbol{l}^{(0)}, t_{u,i}^{(0)}$, maximum of iterations N_{max};
repeat
  Obtain $(\boldsymbol{l}^*, t_u^*, r_0^*, r_u^*)$ by solving Problem (18);
  if $\gamma_u \leq 0$ and $\gamma \leq 0$ **then**
    Set $n = N_{max}$ and update $\boldsymbol{l}^{out} = \boldsymbol{l}^*$;
  else
    Update $\beta_u R_u^{th}$ according to (21);
    Update $R_s(t_{u,i})$ according to (22);
    if Problem (18) is not feasible **then**
      Set $n = N_{max}$ and update $\boldsymbol{l}^{out} = \boldsymbol{l}^{(0)}$;
    end if
  end if
until $n = N_{max}$;
Output: $\boldsymbol{l}^{out}, t_{u,i}^{out}$;

B. IRS Phase Shift Optimization

In this section, IRS's phase shift is optimized with given $\boldsymbol{l}$, $t_{u,i}$, β_u, $\alpha_{u,i}$ and p_i^t. We define

$$\boldsymbol{e}_u(f_i) = \sqrt{p_i^t} g_{u,i} \boldsymbol{e}_{u,r}(f_i)^H \odot \boldsymbol{e}_t(f_i)^T, \boldsymbol{\phi} = [e^{j\phi_1}, \cdots, e^{j\phi_N}]^T,$$

where $\odot$ represents the Hadamard (point-wise) product of two vectors. Then, Problem (13) is simplified to

$$\max_{\boldsymbol{\phi}} \quad R_s(t_{u,i}) \tag{23a}$$
$$\text{s.t.} \quad 0 < \phi_n < 2\pi, 1 \leq n \leq N, \tag{23b}$$
$$|\boldsymbol{e}_u(f_i)\boldsymbol{\phi}|^2 \geq t_{u,i}\sigma_i^2, u \in \mathcal{U}, i \in \mathcal{I}_u. \tag{23c}$$

As (23b) and (23c) are non-convex, Problem (23) is difficult to solve. Define $w_{u,i} = \boldsymbol{e}_u(f_i)\boldsymbol{\phi}$, and function $T_{u,i}(w_{u,i}) = w_{u,i}^2$. As $T_{u,i}(w_{u,i})$ is convex with respect to $w_{u,i}$, its first-order Taylor expansion can be utilized for convex approximation as

$$T_{u,i}(w_{u,i}) \geq T_{u,i}(\hat{w}_{u,i}) + \nabla_{w_{u,i}} T_{u,i}|_{w_{u,i}=\hat{w}_{u,i}}(w_{u,i} - \hat{w}_{u,i}) + \nabla_{w_{u,i}^*} T_{u,i}|_{w_{u,i}=\hat{w}_{u,i}}(w_{u,i}^* - \hat{w}_{u,i}^*). \tag{24}$$

Substituting $w_{u,i} = \boldsymbol{e}_u(f_i)\boldsymbol{\phi}$ and $\hat{w}_{u,i} = \boldsymbol{e}_u(f_i)\hat{\boldsymbol{\phi}}$ into the right hand side of (24), we have

$$T_{u,i}(\boldsymbol{e}_u(f_i)\boldsymbol{\phi}) \geq 2\Re\{\boldsymbol{e}_u(f_i)\hat{\boldsymbol{\phi}}^H \boldsymbol{e}_u(f_i)^H \boldsymbol{\phi}\} - |\boldsymbol{e}_u(f_i)\hat{\boldsymbol{\phi}}|^2. \tag{25}$$

Based on (25), for given $\hat{\boldsymbol{\phi}}$, the convex approximation of Problem (23) can be constructed as

$$\max_{\boldsymbol{\phi}} \quad R_s(t_{u,i}) \tag{26a}$$
$$\text{s.t.} \quad 0 < \phi_n < 2\pi, 1 \leq n \leq N, \tag{26b}$$
$$2\Re\{\boldsymbol{\Theta}_{u,i}(\hat{\boldsymbol{\phi}})\boldsymbol{\phi}\} \geq \Psi_{u,i}(\hat{\boldsymbol{\phi}}), u \in \mathcal{U}, i \in \mathcal{I}_u, \tag{26c}$$

where $\Psi_{u,i}(\hat{\boldsymbol{\phi}}) = |\boldsymbol{e}_u(f_i)\hat{\boldsymbol{\phi}}|^2 + \sigma_i^2 t_{u,i}$, and $\boldsymbol{\Theta}_{u,i}(\hat{\boldsymbol{\phi}}) = \boldsymbol{e}_u(f_i)\hat{\boldsymbol{\phi}}^H \boldsymbol{e}_u(f_i)^H$. However, as (26b) is non-convex, the Lagrangian dual method cannot be applied to solve Problem (26) due to the non-zero dual gap. In the following, we adopt a pricing mechanism to solve Problem (26), where a series of non-negative prices $\{\rho_{u,i}\}$ are introduced for constraints (26c). Then, a penalty term is introduced to the objective function, and Problem (26) is transformed to

$$\max_{\boldsymbol{\phi}} \; R_s(t_{u,i}) + \sum_{u\in\mathcal{U}}\sum_{i\in\mathcal{I}_u} \rho_{u,i}\Big(2\Re\{\boldsymbol{\Theta}_{u,i}(\hat{\boldsymbol{\phi}})\boldsymbol{\phi}\} - \Psi_{u,i}(\hat{\boldsymbol{\phi}})\Big) \quad \text{s.t. } 0 < \phi_n < 2\pi, 1 \leq n \leq N. \tag{27}$$

Given pricing factors $\rho_{u,i}$, the optimal phase of n-th IRS element to Problem (27) is

$$\phi_n^* = \hat{\boldsymbol{\Theta}}_n(\rho_{u,i}), \text{and } \hat{\boldsymbol{\Theta}}(\rho_{u,i}) = \arg\left(\sum_{u\in\mathcal{U}}\sum_{i\in\mathcal{I}_u} 2\rho_{u,i}\boldsymbol{\Theta}_{u,i}^*(\hat{\boldsymbol{\phi}})\right), \tag{28}$$

where $\hat{\boldsymbol{\Theta}}_n(\rho_{u,i})$ is the n-th element of $\hat{\boldsymbol{\Theta}}(\rho_{u,i})$.

If the obtained solution $\boldsymbol{\phi}^*$ is not feasible, the introduced penalty term will reduce the objective value. Consequently, the pricing factors $\{\rho_{u,i}\}$ should be optimized so that the introduced penalty term $\rho_{u,i}\left(2\Re\{\boldsymbol{\Theta}_{u,i}(\hat{\boldsymbol{\phi}})\boldsymbol{\phi}\} - \Psi_{u,i}(\hat{\boldsymbol{\phi}})\right)$ is minimized. Then, to obtain pricing factor $\rho_{u,i}^*$, we employ the sub-gradient descent based method. To be specific, $\{\rho_{u,i}^{(t)}\}$ in the t-th iteration is updated as

$$\rho_{u,i}^{(t)} = \left[\rho_{u,i}^{(t-1)} - \tau_{u,i}^{(t)}\left(2\Re\{\boldsymbol{\Theta}_{u,i}(\hat{\boldsymbol{\phi}})\boldsymbol{\phi}\} - \Psi_{u,i}(\hat{\boldsymbol{\phi}})\right)\right]^+, \tag{29}$$

where $[a]^+ = \max\{0, a\}$, $\tau_{u,i}^{(t)}$ is the positive step-size.

Algorithm 2 Sub-Gradient Descent (SGD) Algorithm

Initialize $\rho_{u,i}^{(0)}$, $\tau_{u,i}^{(0)}$, $\forall u \in \mathcal{U}$, the convergence precision ς and the iteration number $t = 1$;
repeat
  Calculate $\boldsymbol{\phi}^{(t)}$ according to (28);
  Update $\rho_{u,i}^{(t)}$ according to (29);
until $|\boldsymbol{\phi}^{(t)} - \boldsymbol{\phi}^{(t-1)}| \leq \varsigma$.

Proposition 1. *The SGD algorithm can find the globally optimal solution to Problem (26).*

Proof: See Appendix A. □

Problem (23) then can be solved by transforming it into a series of Problem (26), and a sequence of solutions can be obtained by successively solving Problem (26) according to SGD Algorithm.

C. Sub-band Allocation and Power Control Optimization

Given IRS coordinates $\boldsymbol{l}$ and the IRS coefficient $\boldsymbol{\Phi}$, the auxiliary variables, the sub-bands and the power allocation

can be optimized by solving the following problem:

$$\max_{\beta_u, p_i^t, \alpha_u, \delta_{u,i}} \quad R_s(\delta_{u,i}) - W_\beta \sum_{u\in\mathcal{U}} (\beta_u - 1)^2 \tag{30a}$$

$$(13b), (13c), C1 - C2. \tag{30b}$$

Problem (30) turns out to be a conventional sub-band allocation and power control problem, which can be solved by the dual-based method given in [25].

In summary, we propose BCS algorithm to solve Problem (13), and the detailed algorithm is presented in Algorithm 3. The BCS algorithm consists of solving three sub-problems sequentially, i.e., Problem (30), (23) and (14), where the variables can be iteratively optimized while keeping the others fixed. 1) For Problem (30), according to [25], the obtained solution satisfies its Karush–Kuhn–Tucker (KKT) conditions. 2) The IRS phase shift optimization Problem (23) is transformed into a series of approximate Problem (26), which can be optimally solved by the SGD Algorithm. Then, the sequence of solutions to Problem (26) converges to be a local minimum to Problem (23) [26]. 3) For the optimization of IRS's coordinates, the obtained objective value by the RPB algorithm is non-decreasing due to the introduced penalties. Overall, the objective value $R^{(n)}$ is non-decreasing over each iteration, so that the convergence of BCS Algorithm is guaranteed.

Algorithm 3 Block Coordinate Searching (BCS) Algorithm

1: Initialize $\boldsymbol{\phi}^{(0)}$, the convergence precision σ and the iterative number $n = 0$.
2: **repeat**
3: Calculate ${\beta_u}^{(n+1)}$, ${p_i^t}^{(n+1)}$ and $\alpha_{u,i}^{(n+1)}$ by solving Problem (30);
4: Initialize $\hat{\boldsymbol{\phi}}^{(0)} = \boldsymbol{\phi}^{(n)}$, convergence precision ς and iterative number $s = 1$;
5: **repeat**
6: Solving Problem (26) using SGD Algorithm;
7: Formulate Problem (26) with $\hat{\boldsymbol{\phi}}^{(s)} = \boldsymbol{\phi}^{(s)}$;
8: **until** $|\boldsymbol{\phi}^{(s)} - \boldsymbol{\phi}^{(s-1)}| \leq \varsigma$;
9: Set $\boldsymbol{\phi}^{(n+1)} = \boldsymbol{\phi}^{(s)}$,
10: Calculate ${t_{u,i}}^{(n+1)}$, $\boldsymbol{l}^{(n+1)}$ by solving Problem (30) using RPB algorithm
11: Calculate $R^{(n+1)}$ according to (12a);
12: **until** $|R^{(n+1)} - R^{(n)}| \leq \sigma$;

The complexity of the BCS Algorithm consists of three parts: 1) The complexity of the dual-based method in step 3 is $\mathcal{O}(U^4 + U^3 I)$ [25]; 2) The second part is the phase shit optimization in steps 4-9. Let S denote the iteration number in step 8, and the number of iterations in SGD algorithm is T. Then, the complexity to find $\boldsymbol{\phi}^{(n+1)}$ is $\mathcal{O}(ST)$; 3) The last part is the RPB algorithm in step 10. In the worst case, the complexity to find $\boldsymbol{l}^{(n+1)}$ is $\mathcal{O}(QN_{max})$, where Q is the the number of iterations required to solve Problem (18). Let W denote the iteration number in step 12. Then, the total complexity of BCS algorithm is concluded as $\mathcal{O}(W(QN_{max} + ST + U^4 + U^3))$.

V. Simulation Results

In this section, simulation results are presented. UEs are uniformly distributed in a 4 m $\times$ 4 m square area, the ceiling height is 3 m, and the AP is located at $(0, 0, 2)$. The bandwidth of each sub-band is 10 GHz, rate requirement is 40 GHz for each UE, the transmission frequency is 280-360 GHz, $G_t = 20$ dBi, $G_r = 10$ dBi [13] and p_{max} is 20 dBm [27]. All results are obtained by averaging over 100 random realizations of UE locations. The proposed algorithm is labelled as "BCS". We set σ as 10^{-2}, and the maximum number of iterations is restricted to 20 iterations. For comparison, we consider two different cases: 1) The coordinates of the IRS is fixed in the area centre; 2) The phase shift and coordinates of IRS are both fixed. These two cases can be obtained by removing step 10 and steps 4-10 of Algorithm 3, and they are labelled as "LocFix", "IRSFix", respectively.

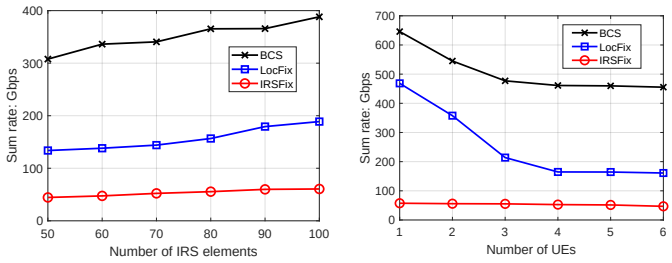

(a) Impact of IRS elements numbers. (b) Impact of the number of UEs.

Fig. 2: Sum-rate performance comparisons.

Fig. 2(a) illustrates the sum-rate performance obtained by different algorithms with the number of UEs $U = 3$. It is observed that the proposed "BCS" algorithm always achieves the best performance. The sum-rates obtained by all considered schemes increase with the number of reflecting elements. This validates that the propagation channel condition can be significantly improved by utilizing the IRS. Fig. 2(b) illustrates the impact of the number of UEs on the sum-rate performance with the number of IRS elements $N = 5\times 20$. As expected, the "BCS" algorithm outperforms the other schemes. The sum-rate decreases with the number of UEs as the rate requirement of each UE needs to be satisfied. Furthermore, the performance gaps between different schemes decrease with the number of UEs. The reason is that UEs are scattered in the simulated area, which makes it more difficult to optimize the communication channel by utilizing the IRS.

Acknowledgments

This work was supported in part by the National Natural Science Foundation of China under Grants 62001107, No. 61971129, No. 61960206005, No. 61871128, Basic Research Project of Jiangsu Provincial Department of Science and Technology under Grant No. BK20190339, No. Bk20192002.

Appendix A
Proof of Proposition 1

The proposition is proved by using contradiction.

Let $\{\rho_{u,i}^*\}$ and $\boldsymbol{\phi}^*(\rho_{u,i}^*)$ denote the converged results obtained by SGD algorithm. We define function $f_{u,i}(\boldsymbol{\phi}^*) = 2\Re\{\boldsymbol{\Theta}_{u,i}(\hat{\boldsymbol{\phi}})\boldsymbol{\phi}^*\} - \Psi_{u,i}(\hat{\boldsymbol{\phi}})$.

Assume that $\boldsymbol{\phi}^*(\rho_{u,i}^*)$ is not the globally optimal solution to Problem (26), so that the constraint (26c) cannot be satisfied for all $u \in \mathcal{U}$. Let $\mathcal{U}_1$ denote the set of UEs that satisfy the constraint (26c), and the set of the left unsatisfied UEs are denoted by $\mathcal{U}_2$, i.e., $\mathcal{U} = \mathcal{U}_1 + \mathcal{U}_2$. Then, denote the globally

optimal solution to Problem (26) as $\tilde{\boldsymbol{\phi}}$, then the following inequalities hold:

$$\sum_{u\in\mathcal{U}_1}\sum_{i\in\mathcal{I}_u}\rho^*_{u,i}f_{u,i}(\boldsymbol{\phi}^*)<0<\sum_{u\in\mathcal{U}_1}\sum_{i\in\mathcal{I}_u}\rho^*_{u,i}f_{u,i}(\tilde{\boldsymbol{\phi}}). \quad \text{(A.1)}$$

Adding the same term to both sides of (A.1), we have

$$S_{\mathcal{U}}<\sum_{u\in\mathcal{U}_1}\sum_{i\in\mathcal{I}_u}\rho^*_{u,i}f_{u,i}(\tilde{\boldsymbol{\phi}})+\sum_{u\in\mathcal{U}_2}\sum_{i\in\mathcal{I}_u}\rho^*_{u,i}f_{u,i}(\boldsymbol{\phi}^*), \quad \text{(A.2)}$$

where $S_{\mathcal{U}}=\sum_{u\in\mathcal{U}}\sum_{i\in\mathcal{I}_u}\rho^*_{u,i}f_{u,i}(\boldsymbol{\phi}^*)$. Meanwhile, as the phase vector $\boldsymbol{\phi}^*$ obtained in Algorithm 2 achieves the globally optimal solution to Problem (27), we have

$$S_{\mathcal{U}}>\sum_{u\in\mathcal{U}}\sum_{i\in\mathcal{I}_u}\rho^*_{u,i}f_{u,i}(\tilde{\boldsymbol{\phi}}). \quad \text{(A.3)}$$

Then, combining (A.2) and (A.3), as well as removing the common terms in $\mathcal{U}_1$, we have

$$\sum_{u\in\mathcal{U}_2}\sum_{i\in\mathcal{I}_u}\rho^*_{u,i}f_{u,i}(\boldsymbol{\phi}^*)>\sum_{u\in\mathcal{U}_2}\sum_{i\in\mathcal{I}_u}\rho^*_{u,i}f_{u,i}(\tilde{\boldsymbol{\phi}}). \quad \text{(A.4)}$$

Then, we consider two cases for $\rho^*_{u,i}$: 1) $\rho^*_{u,i}=0,\ \forall u\in\mathcal{U}_2$; 2) $\rho^*_{u',i}>0, u'\in\mathcal{U}', \mathcal{U}'\subseteq\mathcal{U}_2$ and $i\in\mathcal{I}_{u'}$. In the first case, the left hand side and the right hand side of (A.4) both equal zero, which contradicts the assumption.

In the second case, as $\rho^*_{u',i}>0$ and SGD algorithm is based on the sub-gradient method, then with a sufficient small step size, the converged result $\boldsymbol{\phi}^*$ obtained by SGD algorithm satisfies the condition of $f_{u,i}(\boldsymbol{\phi}^*)=0, \forall u'\in\mathcal{U}', i\in\mathcal{I}_{u'}$. Then, combining with the left hand side of (A.4), we have

$$0>\sum_{u\in\mathcal{U}_2}\sum_{i\in\mathcal{I}_u}\rho^*_{u,i}f_{u,i}(\tilde{\boldsymbol{\phi}}). \quad \text{(A.5)}$$

As $\rho^*_{u',i}>0$, it is inferred that $f_{u,i}(\tilde{\boldsymbol{\phi}})<0, \forall u'\in\mathcal{U}', i\in\mathcal{I}_{u'}$. This contradicts the constraints in (26c). However, as the $\tilde{\boldsymbol{\phi}}$ is the globally optimal solution to Problem (26), so that $\tilde{\boldsymbol{\phi}}$ should satisfy all the constraints of Problem (26). As a result, the assumption does not hold, and $\boldsymbol{\phi}^*(\rho^*_{u,i})$ is the globally optimal solution to Problem (26). Hence, the proof is completed.

REFERENCES

[1] C. Chaccour, M. N. Soorki, W. Saad, M. Bennis, and P. Popovski, "Can terahertz provide high-rate reliable low latency communications for wireless VR?" [Online]. Available: https://arxiv.org/pdf/2005.00536

[2] C. Pan, H. Ren, K. Wang, M. Elkashlan, A. Nallanathan, J. Wang, and L. Hanzo, "Intelligent reflecting surface aided MIMO broadcasting for simultaneous wireless information and power transfer," *IEEE Journal on Selected Areas in Communications*, vol. 38, no. 8, pp. 1719–1734, 2020.

[3] C. Pan, H. Ren, K. Wang, W. Xu, M. Elkashlan, A. Nallanathan, and L. Hanzo, "Multicell MIMO communications relying on intelligent reflecting surfaces," *IEEE Transactions on Wireless Communications*, vol. 19, no. 8, pp. 5218–5233, 2020.

[4] J. Zhang, E. Björnson, M. Matthaiou, D. W. K. Ng, H. Yang, and D. J. Love, "Prospective multiple antenna technologies for beyond 5G," *IEEE Journal on Selected Areas in Communications*, vol. 38, no. 8, pp. 1637–1660, 2020.

[5] W. Chen, X. Ma, Z. Li, and N. Kuang, "Sum-rate maximization for intelligent reflecting surface based terahertz communication systems," in *IEEE International Conference on Communications Workshops in China (ICCC Workshops)*, 2019/8/11 - 2019/8/13, pp. 153–157.

[6] X. Ma, Z. Chen, W. Chen, Z. Li, Y. Chi, C. Han, and S. Li, "Joint channel estimation and data rate maximization for intelligent reflecting surface assisted terahertz MIMO communication systems," *IEEE Access*, vol. 8, pp. 99 565–99 581, 2020.

[7] Z. Wan, Z. Gao, M. Di Renzo, and M.-S. Alouini, "Terahertz massive MIMO with holographic reconfigurable intelligent surfaces." [Online]. Available: https://arxiv.org/pdf/2009.10963

[8] J. M. Jornet and I. F. Akyildiz, "Channel modeling and capacity analysis for electromagnetic wireless nanonetworks in the terahertz band," *IEEE Transactions on Wireless Communications*, vol. 10, no. 10, pp. 3211–3221, 2011.

[9] Z. Wei, Y. Cai, Z. Sun, D. W. K. Ng, J. Yuan, M. Zhou, and L. Sun, "Sum-rate maximization for IRS-assisted UAV OFDMA communication systems," *IEEE Transactions on Wireless Communications*, pp. 1–1, 2020.

[10] T. J. McQueen, C. Della Silva, S. G. Johnston, W. R. Barnett, C. Merrill, and J. C. Couch, "Object tracking and authentication using modular wall units," Feb. 13 2020, US Patent App. 16/362,432.

[11] H. Li, K. Ota, and M. Dong, "Learning IoT in edge: Deep learning for the internet of things with edge computing," *IEEE network*, vol. 32, no. 1, pp. 96–101, 2018.

[12] M. Tao, K. Ota, and M. Dong, "Locating compromised data sources in IoT-enabled smart cities: A great-alternative-region-based approach," *IEEE Transactions on Industrial Informatics*, vol. 14, no. 6, pp. 2579–2587, 2018.

[13] C. Han and I. F. Akyildiz, "Distance-aware bandwidth-adaptive resource allocation for wireless systems in the terahertz band," *IEEE Transactions on Terahertz Science and Technology*, vol. 6, no. 4, pp. 541–553, 2016.

[14] C. Han, A. O. Bicen, and I. F. Akyildiz, "Multi-ray channel modeling and wideband characterization for wireless communications in the terahertz band," *IEEE Transactions on Wireless Communications*, vol. 14, no. 5, pp. 2402–2412, 2015.

[15] E. Basar, M. Di Renzo, J. de Rosny, M. Debbah, M.-S. Alouini, and R. Zhang, "Wireless communications through reconfigurable intelligent surfaces," *IEEE Access*, vol. 7, pp. 116 753–116 773, 2019.

[16] W. Tang, X. Chen, M. Z. Chen, J. Y. Dai, Y. Han, M. Di Renzo, S. Jin, Q. Cheng, and T. J. Cui, "Path loss modeling and measurements for reconfigurable intelligent surfaces in the millimeter-wave frequency band." [Online]. Available: http://arxiv.org/pdf/2101.08607v1

[17] M. T. Barros, R. Mullins, and S. Balasubramaniam, "Integrated terahertz communication with reflectors for 5g small-cell networks," *IEEE Transactions on Vehicular Technology*, vol. 66, no. 7, pp. 5647–5657, 2017.

[18] S. Priebe, M. Kannicht, M. Jacob, and T. Kürner, "Ultra broadband indoor channel measurements and calibrated ray tracing propagation modeling at THz frequencies," *Journal of Communications and Networks*, vol. 15, no. 6, pp. 547–558, 2013.

[19] M. Pengnoo, M. T. Barros, L. Wuttisittikulkij, B. Butler, A. Davy, and S. Balasubramaniam, "Digital twin for metasurface reflector management in 6G terahertz communications," *IEEE Access*, vol. 8, p. 1, 2020.

[20] W. Hao, G. Sun, M. Zeng, Z. Zhu, Z. Chu, O. A. Dobre, and P. Xiao, "Robust design for intelligent reflecting surface assisted MIMO-OFDMA terahertz communications." [Online]. Available: https://arxiv.org/pdf/2009.05893

[21] W. Tang, M. Z. Chen, X. Chen, J. Y. Dai, Y. Han, M. Di Renzo, Y. Zeng, S. Jin, Q. Cheng, and T. J. Cui, "Wireless communications with reconfigurable intelligent surface: Path loss modeling and experimental measurement," *IEEE Transactions on Wireless Communications*, vol. 20, pp. 421–439, 2021.

[22] "Fraunhofer distance," 2019. [Online]. Available: https://en.wikipedia.org/w/index.php?title=Fraunhofer_distance&oldid=888601797

[23] A.-A. A. Boulogeorgos, E. N. Papasotiriou, and A. Alexiou, "A distance and bandwidth dependent adaptive modulation scheme for THz communications," in *IEEE International Workshop on Signal Processing Advances in Wireless Communications (SPAWC)*, 2018/6/25 - 2018/6/28, pp. 1–5.

[24] J. Du, F. R. Yu, and et al., "MEC-assisted immersive VR video streaming over terahertz wireless networks: A deep reinforcement learning approach," *IEEE Internet of Things Journal*, p. 1, 2020.

[25] C. Y. Wong, R. S. Cheng, K. B. Lataief, and R. D. Murch, "Multiuser OFDM with adaptive subcarrier, bit, and power allocation," *IEEE Journal on Selected Areas in Communications*, vol. 17, no. 10, pp. 1747–1758, 1999.

[26] B. R. Marks and G. P. Wright, "Technical note—a general inner approximation algorithm for nonconvex mathematical programs," *Operations Research*, vol. 26, no. 4, pp. 681–683, 1978.

[27] C. Lin and G. Y. Li, "Energy-efficient design of indoor mmwave and sub-thz systems with antenna arrays," *IEEE Transactions on Wireless Communications*, p. 1, 2016.